Journal of Fluids and Structures (2001) **15,** 83–106
doi:10.1006/jfls.2000.0321, available online at http://www.idealibrary.com on IDEAL®

IDENTIFICATION AND PREDICTION OF UNSTEADY TRANSONIC AERODYNAMIC LOADS BY MULTI-LAYER FUNCTIONALS

F. D. MARQUES

Departamento de Engenharia Mecânica, Universidade de São Paulo
Cx. Postal 359, 13560-970 São Carlos, SP, Brazil

AND

J. ANDERSON

Department of Aerospace Engineering, University of Glasgow
Glasgow G12 8QQ, Scotland, U.K.

(Received 25 June 1998, and in final form 22 June 2000)

Nonlinear unsteady aerodynamic effects present major modelling difficulties in the analysis and control of aeroelastic response. A rigorous mathematical framework, that can account for the complex nonlinearities and time-history effects of the unsteady aerodynamic response, is provided by the use of functional representations. A recent development, based on functional approximation theory, has achieved a new functional form; namely, multi-layer functionals. The development of a multi-layer functional for discrete-time, finite memory, causal systems has been shown to be realizable via finite impulse response neural networks. Identification of an appropriate temporal neural network model of the nonlinear transonic aerodynamic response is facilitated via a supervised training process using multiple input–output sets, with data obtained by an Euler CFD code. The training process is based on a genetic algorithm to optimize the network architecture, combined with a random search algorithm to update weight and bias values. The approach is examined for two different multiple aerodynamic input–output data sets, and in both cases, the prediction properties of the network model establish the multi-layer functional as a suitable representation of unsteady aerodynamic response.

1. INTRODUCTION

MODELLING AND PREDICTION of unsteady aerodynamic behaviour presents a significant challenge for the analysis and control of adverse aeroelastic phenomena. In addition, with the enlargement of flight operational conditions in modern aviation, prediction of aeroelastic response can no longer be based on the methodologies that neglect nonlinear effects for describing unsteady aerodynamic behaviour. For unsteady aerodynamic modelling, the nonlinear flow effects of interest are mostly due to separated flows and compressibility effects leading to the appearance and dynamic excursion of shock waves (McCroskey 1977, 1982; Tijdeman & Seebass 1980). As the direct use of the basic fluid mechanic equations (Nixon 1989) is still not practical for aeroelastic applications, approximate models of the nonlinear unsteady aerodynamic response are justified.

Subjected to the premise that the unsteady aerodynamic model can be determined in isolation of the physical laws governing the structural motion, the influence of the implicit

0889–9746/01/010083 + 24 $35.00/0

time-delays on pressure variations introduced by the spatio-temporal propagation and convection of flow variables can be represented by the motion history alone. These assumptions allow the application of the principles of dynamic systems theory, so that unsteady aerodynamic models can be obtained from mathematical laws. Empirical evidence suggests that, for transonic regimes, a functional description of the unsteady aerodynamic force response is justified. The existence of a unique nonlinear aerodynamic force response functional appropriate to a particular flow regime is, necessarily, inferential. Nonuniqueness of the aerodynamic force response is generally associated with certain types of degenerate flowfield behaviour. In particular, aerodynamic hysteresis, flow instability and bifurcation have been identified as key elements in the breakdown of unique, single-valued behaviour of the aerodynamic force response (Tobak & Chapman 1985). Flows admitting shock excursion offer a potentially rich source of mechanisms for the realization of such phenomena. However, computational and experimental evidence suggests that, for certain classes of flows, unique single-valued behaviour of the aerodynamic force response is observed over a range of flow parameters and motion histories. The basic properties of the aerodynamic functional depend on the nature of the flow regime with which it is associated and the class of admissible motion histories for which it is defined.

Tobak and co-workers (Tobak & Pearson 1964; Tobak & Schiff 1981; Tobak & Chapman 1985) have developed a hierarchical class of functional aerodynamic force response models sufficiently general to encompass a broad range of flow regimes and motion histories. Although explicit representation of the aerodynamic force response functional is generally unavailable, its notional existence permits a succinct representation of the aerodynamic force response. In addition, several methods exist to identify approximate aerodynamic force response functionals from known characteristics of the motion history and aerodynamic response.

Other functional forms can also be used to identify nonlinear unsteady aerodynamic models. A convenient approach is based on the Volterra functional series (Silva 1993). In this approach, the functional is approximated by an infinite series of multi-dimensional convolution integrals of increasing order. However, the implementation of these functional forms is generally complicated. In addition, other approaches applied in identification of nonlinear dynamic systems; for example, the Wiener methods and block-oriented models (Billings 1980; Schetzen 1980), present complications for unsteady aerodynamic modelling.

Recently, an alternative approach to the approximation of nonlinear functionals has been proposed by Modha & Hecht-Nielsen (1993), providing an appropriate framework for a large class of nonlinear system models. The so-called, *multi-layer functionals* are a new parametric family of real-valued mappings constructed from a nonlinear combination of linear affine functionals on arbitrary normed spaces. Moreover, the approximate functional form is conveniently represented by a *temporal neural network*. In the context of unsteady aerodynamic response modelling, the use of multi-layer functionals has been firstly applied by Marques & Anderson (1996). The weakly nonlinear behaviour of the normal force coefficient response on pitching 2-D airfoils with mildly trailing edge separated flow has been modelled by a temporal neural network in discrete-time. The approach has shown to be an efficient model form for nonlinear unsteady aerodynamic characteristics. Marques (1997) has formalized the multi-layer functional approach as a representation for the nonlinear unsteady aerodynamic response behaviour for a larger class of flow regimes.

The utility of neural networks in nonlinear system modelling is well-documented (Haykin 1994). Identification of an appropriate temporal neural network model is achieved via a training process, in which a limited sample of system input–output data sets is presented to the network. In general, the network architecture and parameters are adjusted to minimize a measure of the error between the network and the sample outputs. For

a sufficiently broad sample of training data, the inherent generalization properties of the network enable prediction to arbitrary inputs. An advantage of the neural network representation is that it readily accommodates multiple-input/multiple-output system descriptions. In the context of aeroelastic design, a network model of the unsteady aerodynamic response can be combined with a standard structural dynamic model for the purposes of control system design. Furthermore, static freestream parameters (e.g. Mach number) are readily accommodated in the network model thereby ensuring validity over a range of flow regimes.

The present work is concerned with the use of multi-layer functionals in the representation of nonlinear unsteady aerodynamic response. A brief account of the approximation and realization of nonlinear functionals by temporal neural networks is presented. This is followed by a description of a network identification procedure based on a genetic algorithm (Goldberg 1989) combined with a random search algorithm in which both the network architecture and network parameters are optimized for multiple training sets. The genetic algorithm approach has been adopted in order to overcome some of the difficulties of implementing a temporal back-propagation algorithm (Wan 1990). For the particular case of FIR neural networks, the application of a genetic algorithm for training and adaptation provides a more flexible approach. This is a consequence of the ability to assign different time-delays per connection, as well as the absence of causality constraint problems. The approach is tested for two different modelling cases. In both cases, the scheme is used to model the motion-induced unsteady aerodynamic response for a 2-D aerofoil in transonic flow. The first case study considers the aerodynamic responses for a fixed Mach number, while in the second case study a range of Mach numbers is used. The prediction properties of the multi-layer functional representation for both aerodynamic models are presented and discussed.

2. MULTI-LAYER FUNCTIONAL REPRESENTATION

Multi-layer functionals (Modha & Hecht-Nielsen 1993) comprise a new parametric family of real-valued mappings of nonlinear functionals represented as a combination of linear functionals. Multi-layer functionals are defined via an extension of the universal approximator theorem (Cybenko 1989), and are of the general form,

$$\mathscr{MF}[x_t] = \sum_{j=1}^{k} \zeta_j \varphi(\theta_j + \mathscr{L}[x_t]), \tag{1}$$

where ζ_j, $\theta_j \in \Re$, $\mathscr{L}[x_t]$ belongs to the set of all continuous linear functionals on arbitrary normed linear spaces, and k is the number of process units.

Modha & Hecht-Nielsen (1993) have shown that multi-layer functionals can be used as input–output representations for time-invariant, continuous-time, infinite memory, and anti-causal systems. This can be achieved by assuming a basic linear functional, $\mathscr{L}[x_t]$, in the form of a convolution integral, in equation (1). Therefore, a nonlinear dynamic system response, $y(t)$, is approximated by the following functional:

$$y(t) \approx \sum_{j=1}^{k} \zeta_j \varphi\left(\theta_j + \int_0^t h_j(\lambda) x(t-\lambda)\,\mathrm{d}\lambda\right), \tag{2}$$

where ζ_j, $\theta_j \in \Re$, φ is a bounded, continuous function, h_j is the unit impulse response of process unit j due to $x(t)$, for $j = 1, \ldots, k$, and λ is a dummy variable.

2.1. Temporal Neural Networks

A close examination of equation (2) reveals that it corresponds to the definition of *temporal neural networks* (Wan 1990; Haykin 1994). Temporal neural networks comprise the category of neural networks represented by a *spatio-temporal neuron* model joined by connecting links called *synapses*. In this case, the synapses are modelled by *linear*, *time-invariant*, *continuous-time filters*. Each neuron modifies its inputs through an *activation function*.

Figure 1 illustrates the temporal neuron model, in which the synapse i belonging to the neuron j has its temporal behaviour described by an impulse response $h_{ji}(t)$. For the input $x_i(t)$ denoting the excitation applied to synapse i (for $i = 1, \ldots, p$), the synaptic response is determined by the convolution of the impulse response $h_{ji}(t)$ with $x_i(t)$. For a neuron j with a total of p synapses, the associated *activation potential* $v_j(t)$, due to the combined effect of the inputs and the biases θ_j, is given by

$$v_j(t) = \theta_j + \sum_{i=1}^{p} \int_0^t h_{ji}(\lambda) x_i(t - \lambda)\, \mathrm{d}\lambda. \tag{3}$$

The neuron output $y_j(t)$ is obtained by applying the *activation function*, φ (e.g. a sigmoidal function) on $v_j(t)$; that is,

$$y_j(t) = \varphi(v_j(t)). \tag{4}$$

A multi-layer temporal neural network is formed by composing layers of neurons. A schematic representation of a multi-layer network architecture, for the input-output pair $(x(t), y(t))$, composed of neurons modelled by equations (3) and (4), distributed in two hidden

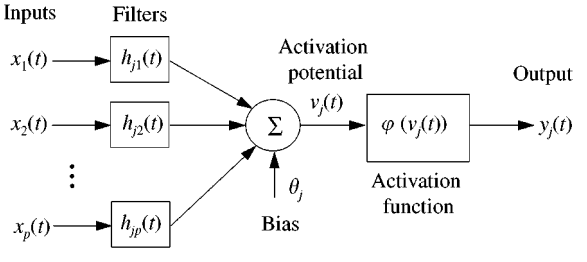

Figure 1. Temporal neuron model.

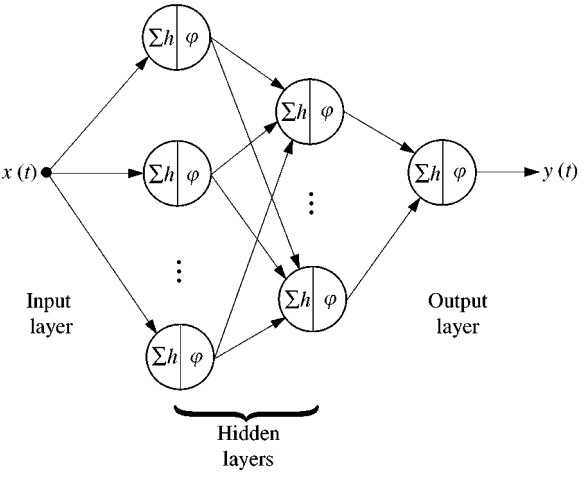

Figure 2. Temporal network architecture.

layers, is depicted in Figure 2. Here each of the neurons are presented as simplified representations of that shown in Figure 1.

2.2. FIR Neural Network Model

From a computational point of view, it is convenient to assign a finite memory T to the synaptic filter and to approximate the convolution integral in equation (3) by a convolution sum. Consequently, the continuous-time variable t is replaced by a discrete-time variable n defined by $t = n\Delta t$, where n is an integer and Δt is the sample interval. Equation (3) is then approximated as

$$v_j(n) = \theta_j + \sum_{i=1}^{p} \sum_{\ell=0}^{\tau_{ji}} w_{ji}(\ell) x_i(n-\ell), \tag{5}$$

where τ_{ji} is the number of delay units of the filter in synapse i belonging to the neuron j, and $w_{ji}(\ell)$ is a weight value at time-delay ℓ.

Equation (5) describes the expression for the activation potential of the *finite impulse response* (FIR) *neuron model*. The neural network model composed of FIR neurons is referred to as a FIR neural network.

3. FIR NETWORK MODEL IDENTIFICATION VIA SUPERVISED TRAINING

Identification of an appropriate FIR network model is achieved via a supervised training process in which a limited sample of system input–output sets is presented to the network. Where the network architecture and network delays are prescribed, the synaptic weights can be trained using a temporal version of the back-propagation algorithm (Haykin 1994; Wan 1990). However, prescribed networks of this kind may exhibit poor generalization properties. An efficient network optimization scheme can be formulated via a genetic algorithm (Goldberg 1989).

Genetic algorithms are a type of evolution-based search algorithm which manipulate sets of possible encoded solutions for a problem. The elements of a conventional genetic algorithm comprise: *Individuals*, representing possible solutions to a problem, with features encoded in a chromosome; *Chromosomes*, the basic units of a genetic algorithm that encode how each individual is to be constructed; *Genes*, subsets of a chromosome that maintain a particular feature of an individual; *Population*, a complete set of individuals; *Fitness Function*, a value assigned to determine how good an individual is as a solution to the given problem.

A genetic algorithm (Goldberg 1989) generally starts with a randomly initialized population. Each individual is evaluated by decoding its chromosome and applying the fitness function. New individuals are the result of combining individuals from the original population. A genetic algorithm is facilitated by the operations of: *Selection*, to choose the individuals for combination; *Crossover*, to create new individuals by swapping genes from the selected individuals; *Mutation*, to guarantee that occasionally (with low probability value) a few genes are modified and therefore a new search space can be explored, thereby increasing the chance of achieving the global minimum. The process is repeated until a new complete population is established, therefore, completing a *generation*. The algorithm is further iterated only if a termination criterion is not satisfied.

The genetic algorithm is used as part of a supervised training process to obtain an optimal architecture for the FIR network while, simultaneously, identifying the synaptic

weights. To achieve this, the algorithm interprets each FIR neural network as an individual belonging to a population. The associated chromosome is a sequence comprising the time-delays and weights per connection. The measure of the network fitness, f, is defined by the inverse of the sum of squared errors between the desired and the network outputs; that is,

$$f = \left(\sum_{i=1}^{N_c} \sum_{n=1}^{L} [d_i(n) - y_i(n)]^2 \right)^{-1}, \tag{6}$$

where N_c is the number of input–output training sets, L is the total number of time samples per training set, $d_i(n)$ is the desired output of training set i at discrete-time n and $y_i(n)$ is the corresponding network output.

The inclusion of multiple data sets in the definition of the network fitness function differs from normal practice where a single (extended) data set is commonly adopted. The main advantage of the present approach lies in the exposure of each of the networks in the population to a broad class of input history, thereby ensuring good generalization properties. The networks in the population are constrained to maintain certain basic features; that is, they must present a multi-layered architecture of biased neurons without missing connections between hidden layers, all hidden neurons are nonlinear (sigmoid activation function), and all output neurons are linear.

The chromosome is represented by a string of constant length irrespective of the architecture encoded within it. This is achieved by assuming an FIR network architecture with bounded parameters. The chromosome size depends on the limiting FIR network considered. It is a string which records the information necessary to decode any feasible network within the pre-defined bounded architecture. For each neuron of the limiting architecture, the string is the sequence of all time-delay values of the previous hidden layer to the neuron itself. The complete chromosome is the sequence described above for all neurons of the limiting architecture. Figure (3) depicts a generic representation for the chromosome encoding FIR networks, where N_i^f is a flag indicating whether the neuron i exists or not, $\tau_{i,j}$ is the time-delay in the connection between neurons j (in the previous layer) to i, and m is the number of neurons of the previous layer.

For each existent neuron, the respective weight vector (for each connection) and the bias value are recorded separately, but they must always be related to their respective connection and neuron, whatever be the genetic operation.

3.1. Network Training Process

The supervised training process commences with an initial population of individuals. Each individual is created with a randomly generated architecture and receives random weight values from a uniform distribution ($-1{\cdot}0$ to $1{\cdot}0$). The entire population is evaluated by a feedforward pass of each individual to produce a fitness distribution.

In the next step, parents are selected using the minimum, average and maximum fitness values in the distribution. The selection operator re-scales the fitnesses of the population via

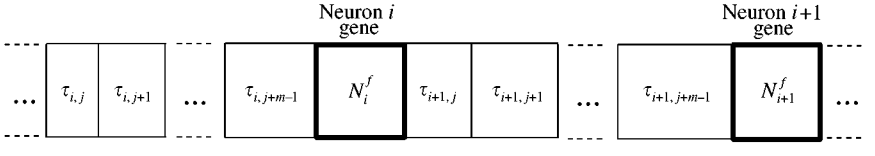

Figure 3. Generic representation of the chromosome.

a linear rule and then conventional roulette wheel selection (Goldberg 1989) is applied. Selected parents produce new individuals by the crossover operator. A crossover operator is used in which multiple crossover points may be chosen. Some care must be taken after the production of new individuals. Encoded FIR networks of different architectures may present problems during genetic operations. The gaps left inside the chromosomes by nonexistent neurons or connections may lead to an inconsistent new individual after the crossover operation. The procedure is monitored to identify potential anomalies. An attempt is made to correct any distortions of the new individuals' architecture thereby enabling chromosome strings to be re-arranged in the best way possible. If this is not feasible, then the new individual is discarded. If a new individual is accepted, there is also a possibility of that individual being mutated. The new individual's chromosome is swept gene by gene and for each gene the mutation operator changes its value with respect to a low probability value. Only time-delay values and neuron genes are mutated (with probability values P_t and P_n, respectively).

A final operation is applied to update weight and bias values of the new individuals. This operation consists of perturbing each weight and bias value by a zero mean, unit variance normally distributed random value scaled by a proportionality constant β. The new values of weight and bias are only accepted if they lead to a fitter network. This process is repeated several times before returning the modified individual to the population.

Following each generation, the new and old individuals are compared in terms of their fitness values and the best individuals are retained for the next generation. To mitigate against the possibility of convergence to sub-optimal solutions, an additional mutation operator is used. This so-called *forced mutation* operator is invoked only after a pre-defined number of generations with the same fitness value for the best individual. For each member of the population, the operator randomly selects a gene which is to be modified. The gene is modified and the individual is tested to check if its new fitness is greater than the old one. If this is the case, the individual is accepted, otherwise it is only accepted with a probability of 10^{-4}. The routine is repeated a number of times and the final mutated individual returns to the population.

Two alternative criteria are used to terminate the genetic algorithm: (i) the number of generations exceeds a pre-defined limit, or (ii) the fitness of the best individual exceeds a pre-defined goal value.

4. MULTI-LAYER FUNCTIONAL OF NONLINEAR UNSTEADY TRANSONIC AERODYNAMIC RESPONSE

To illustrate the use of the multi-layer functional representation in the context of unsteady aerodynamic response modelling, the unsteady aerodynamic response of a 2-D aerofoil to variations in angle of incidence is considered for a range of Mach numbers in the transonic regime. Here, the nonlinear functional relationship (cf. Figure 4) between lift force coefficient $C_L(t)$, pitch moment coefficient at $\frac{1}{4}$ chord length $C_{m_{1/4}}(t)$, and incidence histories α_t, for a NACA-0012 aerofoil operating in a range of Mach numbers is

$$\begin{Bmatrix} C_L(t) \\ C_{m_{1/4}}(t) \end{Bmatrix} = \mathscr{MF}[\alpha_t, M]. \tag{7}$$

Multi-layer functional models are identified for two different problems. The first one considers the identification of a FIR network model for the motion-induced aerodynamic system response described above at a fixed Mach number, while the second problem considers the model identification for a range of Mach numbers ($0{\cdot}625 < M < 0{\cdot}725$). The

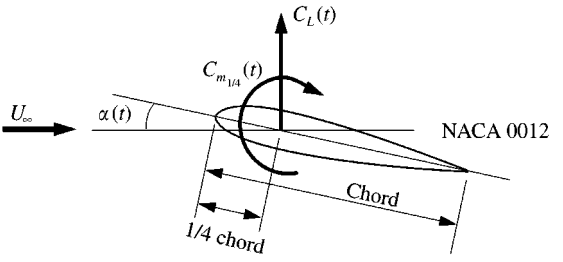

Figure 4. Features for the unsteady aerodynamic response modelling (sonic speed is 340·5 ms^{-1}, and chord length is 0·55 m).

transonic aerodynamic database is created using a CFD code (Dubuc *et al.* 1997) based on the numerical solution of the nonlinear Euler equations. Numerical experiments have been carried out to establish the range of incidence motion which covers the nonlinear behaviour of the aerodynamic response. These experiments are based on the observations of variations of the pressure coefficient distribution around the aerofoil due to shock waves excursion during the incidence motion. For the Mach numbers 0·625, 0·675, and 0·725, the maximum absolute values of the incidence angle that exhibits the aforementioned compressibility effects are, respectively: 4·5, 3·0, and 1·5°. Beyond these values, the data validity produced by the Euler CFD code may be compromised (shock-induced separation may be present and the code does not account for viscous effects).

The training process demands that a broad range of motion-induced unsteady aerodynamic responses be used during the nonlinear identification of the multi-layer functional model. This requirement is associated with the nonlinear nature of the unsteady transonic aerodynamic response, and the need for a variety of characteristic motion histories and Mach numbers within the chosen range for the network identification process. Here, three characteristic motions comprising sinusoidal, ramp-up, and pulse-down input histories are considered in both case studies. The characteristic motions are not derived from of any systematic procedure, but are assumed to explore a sufficiently broad range of the input and output spaces for which a reasonably smooth (transient) unsteady aerodynamic response can be assumed. Another aspect is related to the frequency content of these characteristic motions, that should allow a broad range of frequencies to be captured by the FIR network during the identification process.

To compose the training sets, each characteristic motion is assumed for the respective Mach number, depending on the case study in question. In the first case study, the training patterns are considered at a fixed Mach number value of $M = 0{\cdot}65$, while in the second case study, the training patterns are prescribed at each of the three Mach numbers of 0·625, 0·675, and 0·725, and conform to the limits for the absolute values of incidence. In each training pattern, the motion history is normalized with respect to the maximum incidence prior to training. For all training sets, the appearance and dynamic motion of shock waves responsible for nonlinear behaviour of the unsteady aerodynamic response can be observed. The characteristic motions for training have a sample interval of 0·002 s, to ensure an adequate representation of the input motion histories and output aerodynamic responses.

4.1. First Case Study: Fixed Mach Number

Table 1 presents a description of each one of the training sets used in the identification process. In order to help the convergence, the training process is carried out in stages, with some training parameters altered from one stage to another. A trial-and-error approach is

TABLE 1
Training set motions for the identification of the unsteady aerodynamic response model in the transonic regime (fixed $M = 0{\cdot}65$)

Characteristic motion	Range
Sinusoidal	$\alpha_{mean} = 0^\circ$; amplitude $= 4^\circ$, $k = 0{\cdot}07807$
Sigmoidal ramp-up	$\alpha_{min} = -1^\circ$; $\alpha_{max} = 4^\circ$
Pulse-down	$\alpha_{initial} = 1^\circ$; $\alpha_{pulse} = -4{\cdot}5^\circ$; $\alpha_{final} = 1^\circ$

TABLE 2
Training parameters—first case study

Training parameters	Value		
	Stage 1	Stage 2	Stage 3
Population size	14	14	14
Crossover points	13	13	13
P_t and P_n	0·5%	0·5%	0·5%
β	0·0001	0·0001	0·001
Cycles to update weight/bias	5	5	5
Steps before forced mutation	200	100	100
Generations	100000	100000	50000

used to obtain new training values for each stage. Here, a three-stage training process, totaling 250 000 generations, is carried out. For the maximum complexity FIR network architecture in the population: two hidden layers and 10 neurons per hidden layer are used. The number of hidden layers and number of neurons per hidden layer adopted are based on the typical values for neural networks architectures (Haykin 1994). A maximum time-delay per connection of 6 is assumed (via a trial-and-error approach). Table 2 presents the complete set of training parameters.

The architecture and time-delay distribution of the identified FIR network model is shown in Figure 5. Figures 6–8 present a comparison between the lift force coefficient and pitch moment coefficient responses obtained by the Euler CFD code and the respective FIR network outputs for each of the training sets after the completion of identification process. Figure 9 shows the pressure distribution variation due to the aerofoil motion defined by the case of Figure 6. Here, it is possible to observe the appearance and dynamic motion of the shock wave. The extent of the shock excursion determines the degree of nonlinearity considered in the present work. The generalization properties of the identified FIR network model are examined in Figures 10–15, by presenting arbitrary incidence motion histories to the identified model and comparing Euler CFD code and FIR network outputs.

4.2. SECOND CASE STUDY: RANGE OF MACH NUMBERS

Three characteristic incidence motion histories are also considered in this problem, but here each one is considered at a different Mach number. The training sets are presented in Table 3, and the basic problem features are the same as in Figure 4. A three-stage training process, totaling 430 000 generations, is carried out. For the maximum complexity network architecture in the population, two hidden layers and 10 neurons per hidden layer are used. A maximum time-delay per connection of 4 is assumed. The methodology for selecting the architecture and time-delay values follows a similar approach to that adopted in the first case study. Table 4 presents the complete set of training parameters.

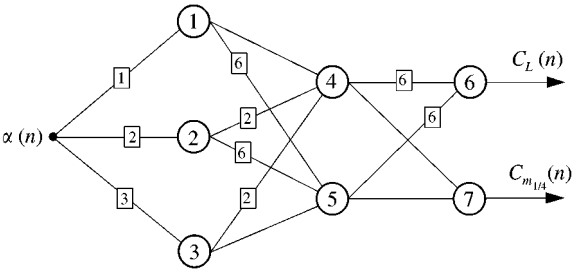

Figure 5. Identified FIR network model for the first case study; fixed M (numbers in the boxes represent time-delays).

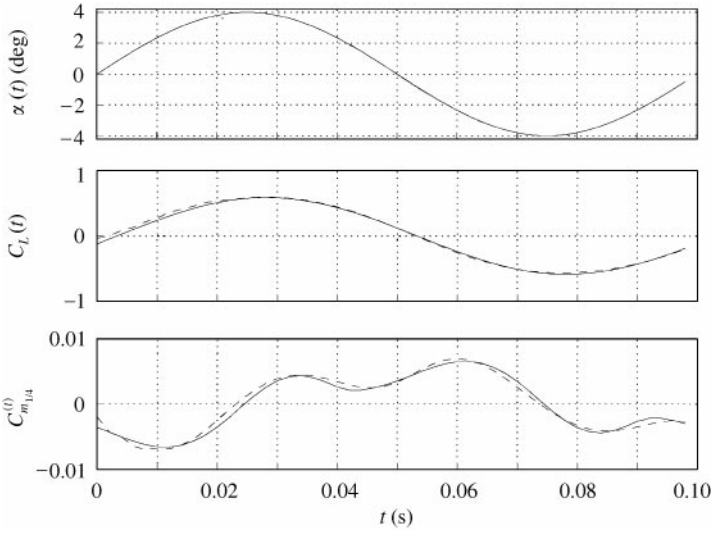

Figure 6. Identification of the unsteady aerodynamic response model in the transonic regime (fixed $M = 0{\cdot}65$, $k = 0{\cdot}07807$): ——, Euler CFD code; – – –, FIR network output, after training for the sinusoidal case.

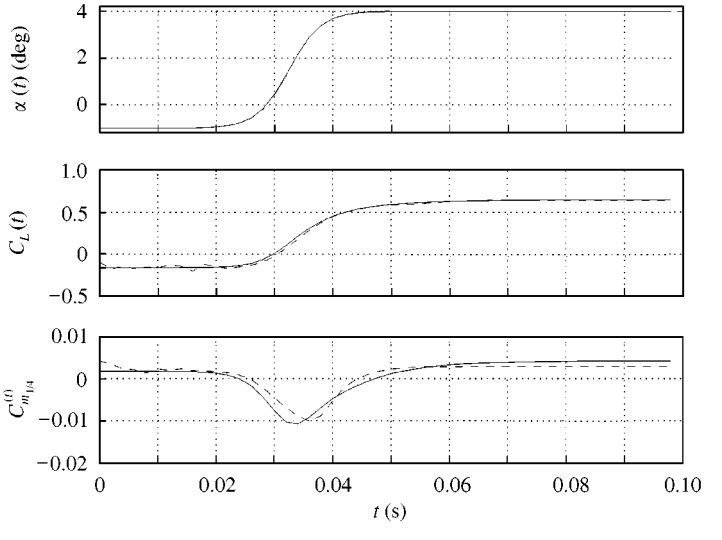

Figure 7. Identification of the unsteady aerodynamic response model in the transonic regime (fixed $M = 0{\cdot}65$): ——, Euler CFD code; – – –, FIR network output, after training for the sigmoidal ramp-up case.

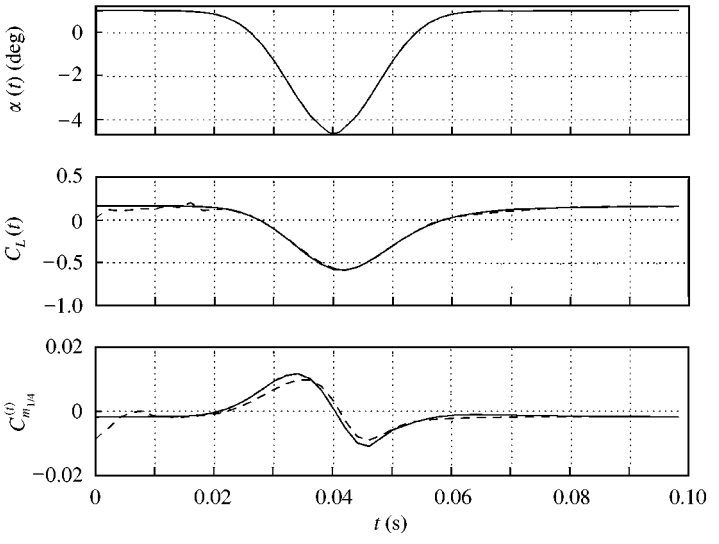

Figure 8. Identification of the unsteady aerodynamic response model in the transonic regime (fixed $M = 0{\cdot}65$): ——, Euler CFD code; – – –, FIR network output, after training for the pulse-down case.

The architecture and time-delay distribution of the identified FIR network model is shown in Figure 16. The training results, after completion of the identification process, are presented in Figures 17–19. Due to the large number of sets (nine in total) only few representative training cases are presented. All the presented motion-induced aerodynamic responses for each transonic Mach number are reasonably reconstructed.

In a similar manner to first case study, the robustness of the identified multi-layer functional model is examined in Figures 20–27 by presenting arbitrary incidence motion histories to the identified model and comparing Euler CFD code and FIR network outputs.

4.3. Discussion

Both unsteady transonic aerodynamic response models have shown encouraging results to endorse the use of multi-layer functional representations. The ability of the FIR network model to capture the essential characteristics of both linear and nonlinear aerodynamic behaviour can be observed in simulations for motion histories (and Mach numbers) different from those used for training purposes. In contrast to the time demanded by the training process to identify the model, evaluations of the resulting network after training are fast enough to allow real-time predictions, justifying further applications in aeroelastic analysis and control design. Moreover, the implementation of a FIR network is simple.

The presence of two hidden layers in both final network models ensures functional complexity, as observed in Figures 5 and 16. The typical time-delay distribution within the network also provides features to the identified models that are consistent with the physical behaviour of unsteady transonic flowfields. Despite the complexity of the searching space, the resulting FIR network architecture is shown to be simple. The simplicity of the architecture, in association with good generalization results, reinforces the satisfactory performance of the identification process. The large number of evaluations required by the training process was due to two main factors: (i) the length of the chromosome to encode the FIR network was relatively large; (ii) the genetic search was carried out in a search space determined by real-valued parameters (network weights per connection).

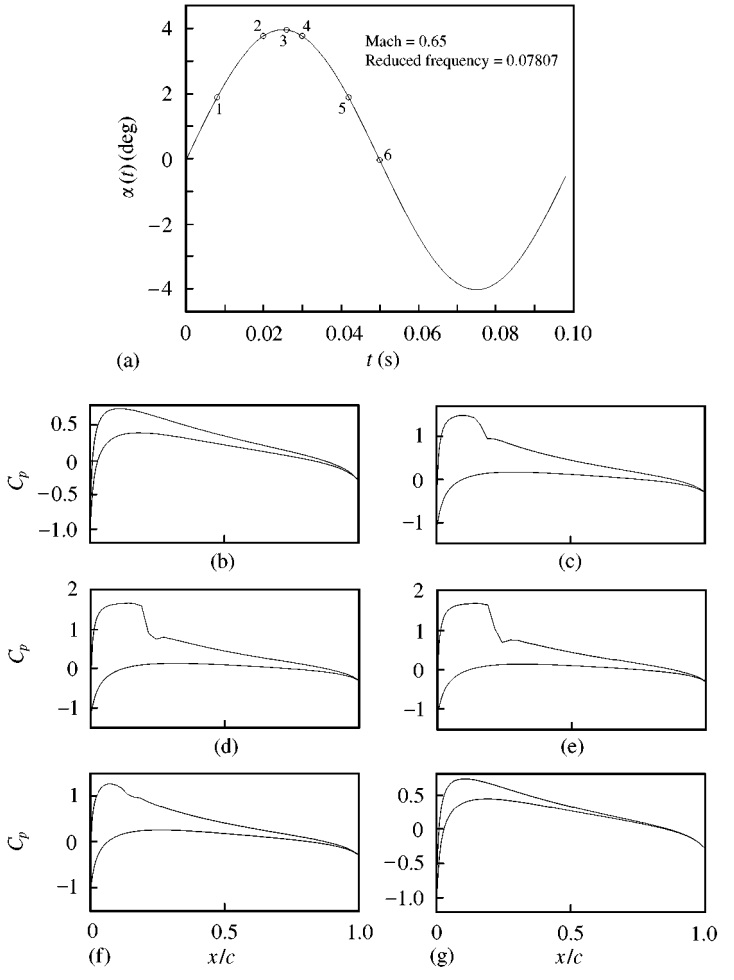

Figure 9. Pressure distribution variation in relation to airfoil motion; Case in Figure 6 ($M = 0{\cdot}65$, $k = 0{\cdot}07807$): (a) angle of attack history; (b) Point 1 at $t = 0{\cdot}008$ s, $\alpha(t) = 1{\cdot}927^\circ$; (c) Point 2 at $t = 0{\cdot}02$ s, $\alpha(t) = 3{\cdot}8^\circ$; (d) Point 3 at $t = 0{\cdot}026$ s, $\alpha(t) = 3{\cdot}99^\circ$; (e) Point 4 at $t = 0{\cdot}03$ s, $\alpha(t) = 3{\cdot}8^\circ$; (f) Point 5 at $t = 0{\cdot}042$ s, $\alpha(t) = 1{\cdot}927^\circ$; (g) Point 6 at $t = 0{\cdot}05$ s, $\alpha(t) = 0{\cdot}0^\circ$.

For the identified FIR network model at fixed Mach number (first case study) the nonlinear behaviour of both lift force and pitch moment coefficients is adequately captured. Some discrepancies are associated with the pitch moment coefficient response; however, these are explained by the more severe nonlinear characteristics of the pitch moment response. Nevertheless, the predicted FIR network response displays the main features of the pitch moment response. For the lift force coefficient, good agreement with the training sets is achieved.

Generally, the predictive capabilities of the identified model of the unsteady aerodynamic response in the transonic regime (for the first case study) are shown to be satisfactory for the majority of the test cases not contained in the training sets. This is particularly true for the lift force coefficient responses. When tested in the linear range of the unsteady aerodynamic response, the identified FIR network model has not shown good predictive qualities, although the error in the overall responses is not patircularly large. The case illustrated in Figure 10 is obtained from a sinusoidal incidence motion with mean angle of attack equal to

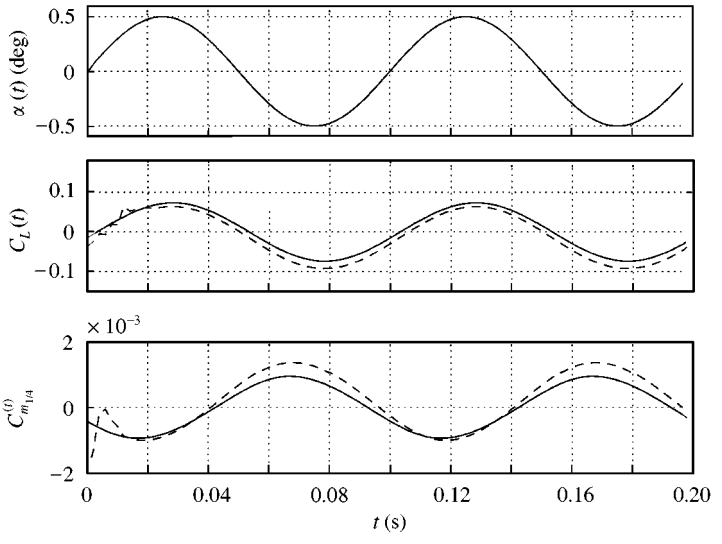

Figure 10. Generalization test of the FIR network model to arbitrary motion history (linear case, $k = 0{\cdot}07807$).: ——— Euler CFD code; – – – FIR network output.

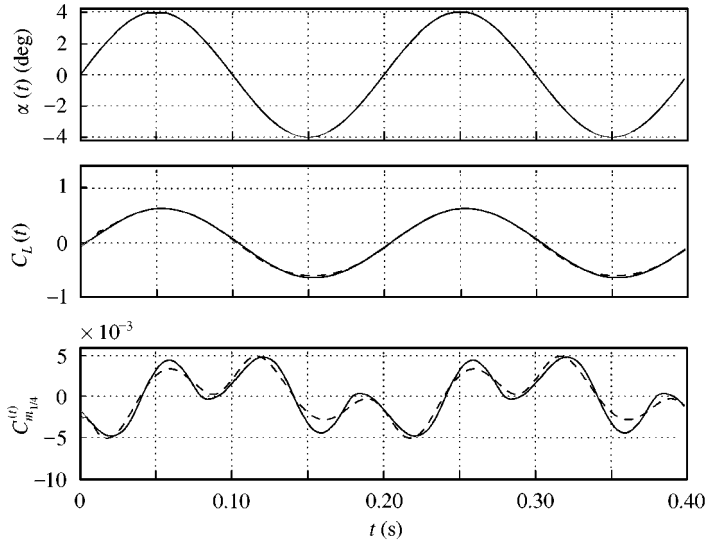

Figure 11. Generalization test of the FIR network model to arbitrary motion history (low-frequency case, $k = 0{\cdot}03903$): ——— Euler CFD code; – – – FIR network output.

zero and 0·5° amplitude at the reduced frequency of 0·07807. The poorer prediction performance compared to the linear case is due to the fact that the training patterns used to achieve the network model are all in the nonlinear range of the unsteady aerodynamics. To reduce this deficiency, a larger set of training patterns is necessary.

In the nonlinear range of the motion-induced unsteady aerodynamic responses, the FIR network model presents good generalization for low-frequency oscillatory cases. Figure 11 presents a case where the sinusoidal incidence motion is half the frequency of the corresponding case used in the training sets. Only a few discrepancies can be observed in the pitch moment response of the FIR network model. Nevertheless, when a higher frequency

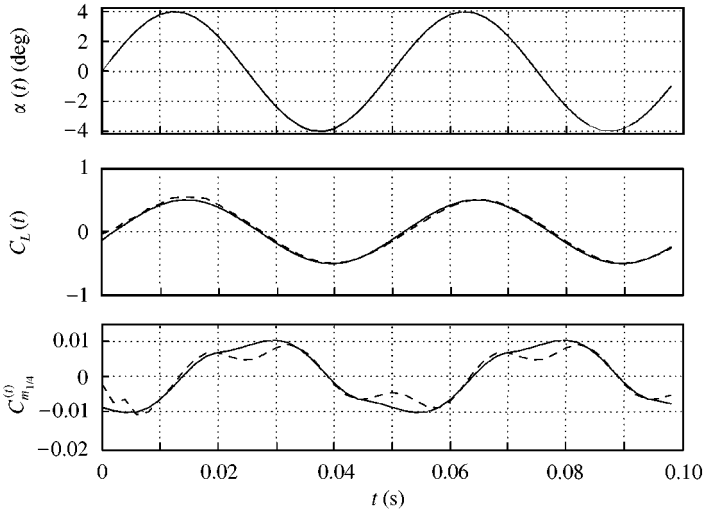

Figure 12. Generalization test of the FIR network model to arbitrary motion history (high-frequency case, $k = 0{\cdot}156$): ——— Euler CFD code; – – – FIR network output.

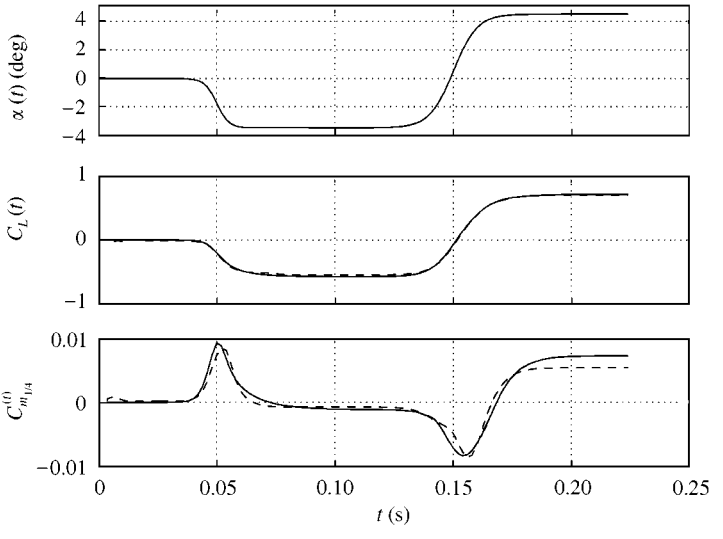

Figure 13. Generalization test of the FIR network model to arbitrary motion history: ——— Euler CFD code; – – – FIR network output.

sinusoidal motion is tested, as in the case illustrated in Figure 12, the discrepancies in the pitch moment response increase. Here, the frequency of the incidence motion is twice that of the corresponding case used in the training sets.

Figures 13–15 present more generalization tests of the first case study FIR neural network model of unsteady aerodynamic response in the transonic regime (fixed $M = 0{\cdot}65$). The FIR network model outputs for those cases also indicate good agreement with the desired unsteady aerodynamic responses, even when the incidence variations are beyond the training limits. In some simulations of the FIR network representation, the unsteady aerodynamic responses present pronounced oscillatory behaviour at the beginning of the motion. The reason for this behaviour is the inherent temporal network transient response

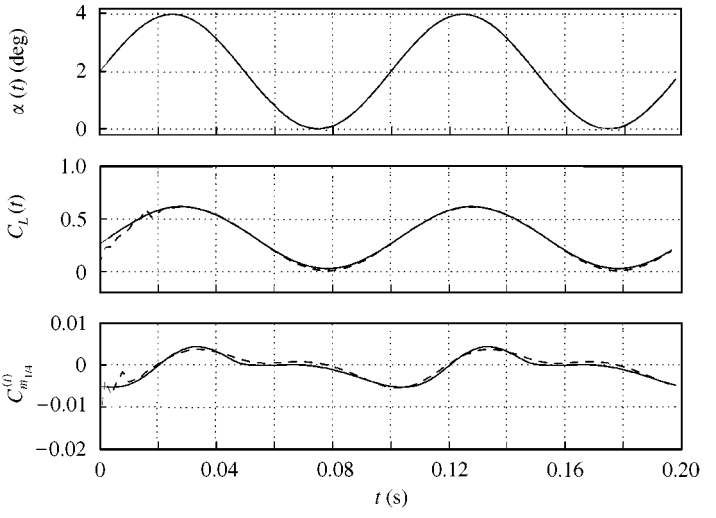

Figure 14. Generalization test of the FIR network model to arbitrary motion history ($k = 0{\cdot}07807$): ——— Euler CFD code; – – – FIR network output.

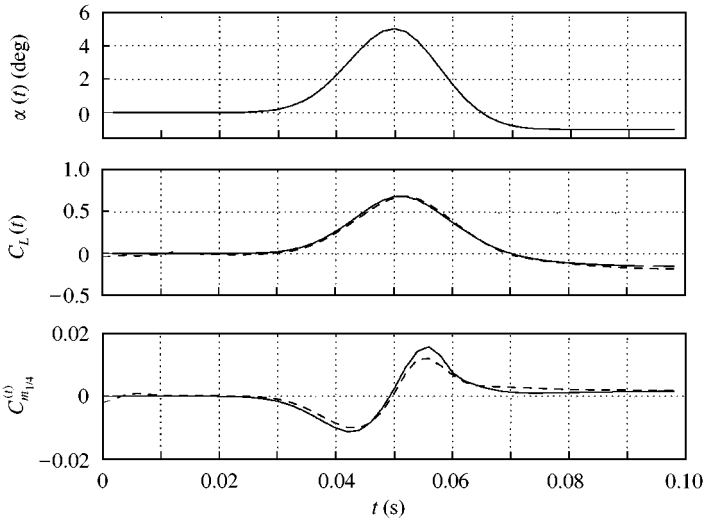

Figure 15. Generalization test of the FIR network model to a motion history beyond the training limits: ——— Euler CFD code; – – – FIR network output.

caused by the absence of time-delay information at the beginning of the motion. In the first steps during the FIR network simulation there is a lack of input information prior to time zero, and the network response is degraded. Therefore, the first steps of the network simulation should be neglected in any discussion of the network prediction qualities.

Significant discrepancies arise again in the pitch moment responses in relation to the lift responses. One can observe that the lift coefficient response is always better predicted by the network model. An explanation is in the different degrees of nonlinearity and time-delay dependency between the two loads. These peculiarities raise difficulties to simultaneously predict both lift and pitch moment coefficient responses with the same level of accuracy. To ensure more accurate predictions of the pitch moment coefficient response, two alternatives

TABLE 3
Training set motions for the identification of the unsteady aerodynamic response model for a range of Mach numbers in the transonic regime

Characteristic motion	M	Range
Sinusoidal	0·625	$\alpha_{mean} = 0°$; amplitude $= 4{\cdot}5°$, $k = 0{\cdot}08119$
	0·675	$\alpha_{mean} = 0°$; amplitude $= 3{\cdot}0°$, $k = 0{\cdot}07517$
	0·725	$\alpha_{mean} = 0°$; amplitude $= 1{\cdot}5°$, $k = 0{\cdot}06999$
Sigmoidal ramp-up	0·625	$\alpha_{min} = 0°$; $\alpha_{max} = 4{\cdot}5°$
	0·675	$\alpha_{min} = 0°$; $\alpha_{max} = 3{\cdot}0°$
	0·725	$\alpha_{min} = 0°$; $\alpha_{max} = 1{\cdot}5°$
Pulse-down	0·625	$\alpha_{initial} = 0°$; $\alpha_{pulse} = -4{\cdot}5°$; $\alpha_{final} = 0°$
	0·675	$\alpha_{initial} = 0°$; $\alpha_{pulse} = -3{\cdot}0°$; $\alpha_{final} = 0°$
	0·725	$\alpha_{initial} = 0°$; $\alpha_{pulse} = -1{\cdot}5°$; $\alpha_{final} = 0°$

TABLE 4
Training parameters—second case study

Training parameters	Value		
	Stage 1	Stage 2	Stage 3
Population size	14	14	14
Crossover points	7	13	5
P_t and P_n	0·5%	0·5%	0·5%
β	10^{-4}	10^{-4}	10^{-4}
Cycles in updating weights	5	5	5
Steps before forced mutation	200	200	100
Generations	200 000	50 000	180 000

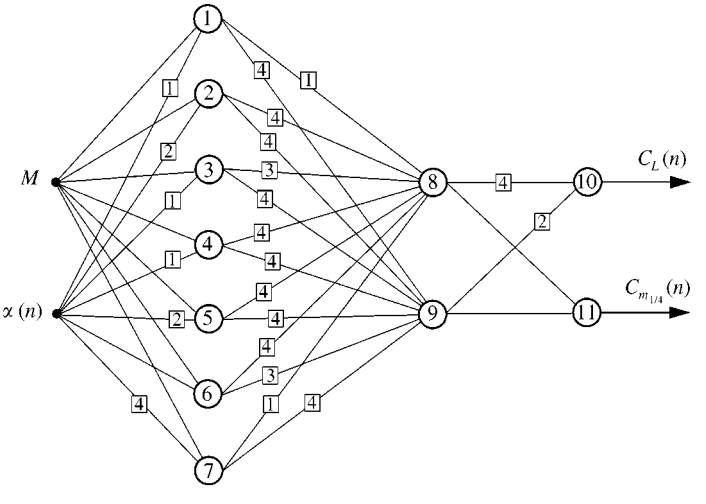

Figure 16. Identified FIR network model for the second case study; range of M (numbers in the boxes represent time-delays).

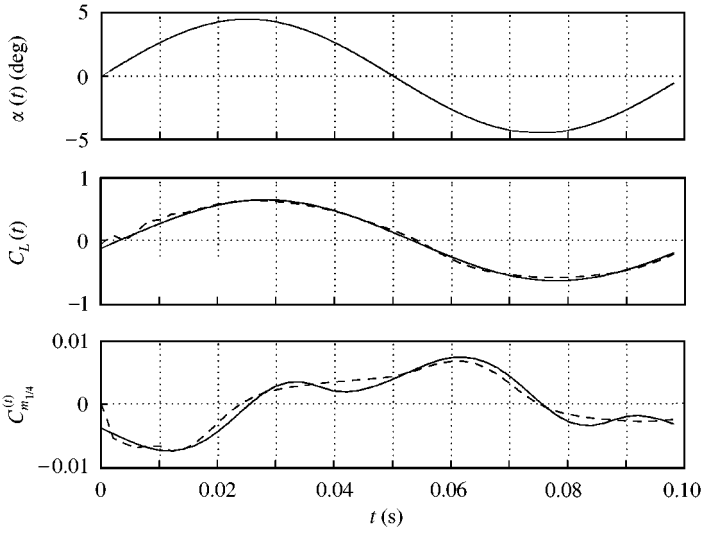

Figure 17. Identification of the unsteady aerodynamic response in the transonic regime ($M = 0{\cdot}625$, $k = 0{\cdot}08119$): ——, Euler CFD code; – – –, FIR network output, after training for the sinusoidal case.

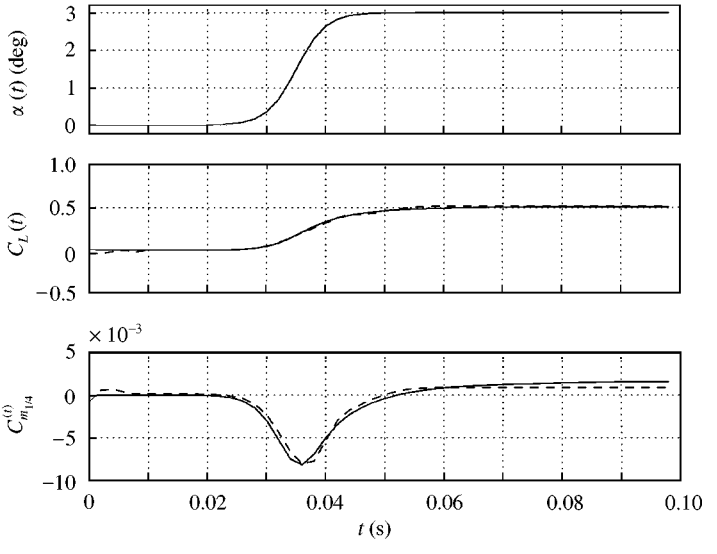

Figure 18. Identification of the unsteady aerodynamic response in the transonic regime ($M = 0{\cdot}675$): ——, Euler CFD code; – – – –, FIR network output, after training for the sigmoidal ramp-up case.

can be suggested. The first approach is to represent lift and pitch moment coefficients by different FIR neural networks, while the second approach is to enlarge the size of the training sets.

The second study case, where a range of M is considered, represents a greater challenge to the identification process. The increased size of the search space, in comparison with the previous case, requires a greater number of training iterations. These difficulties are also observed in the complexity of the final adapted architecture, as depicted in Figure 16. Although discrepancies in the training results for the pitch moment are larger than in the

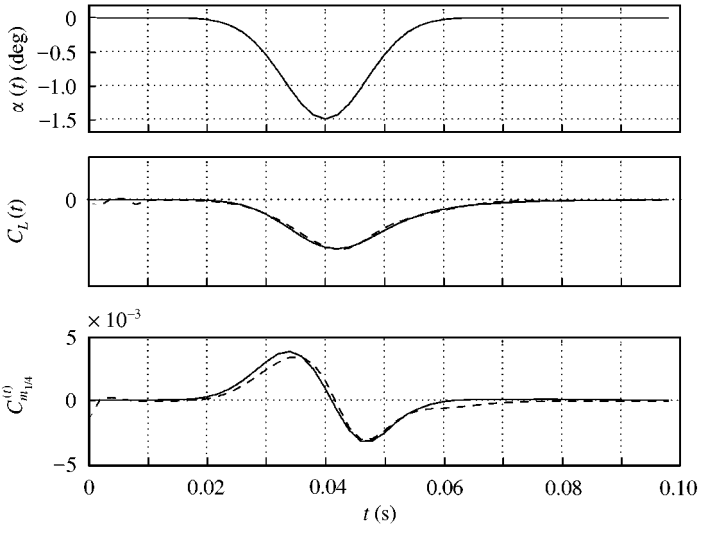

Figure 19. Identification of the unsteady aerodynamic response in the transonic regime ($M = 0{\cdot}725$):——, Euler CFD code; – – –, FIR network output, after training for the pulse-down case.

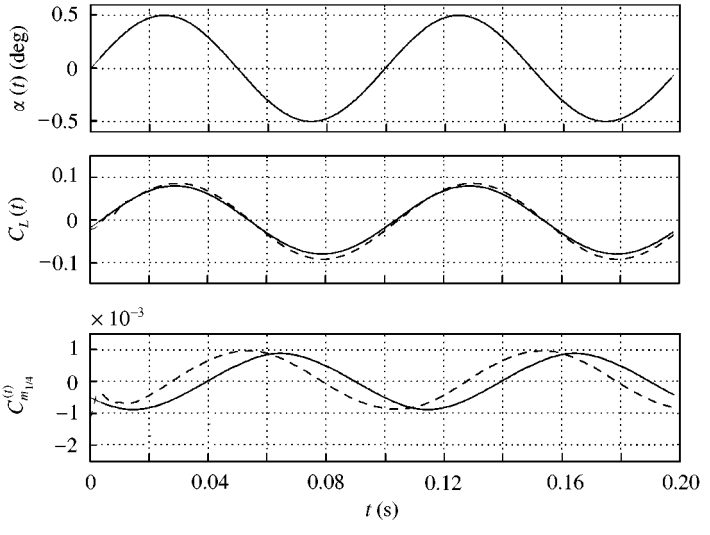

Figure 20. Generalization test of the FIR network model to arbitrary motion history (linear case, $M = 0{\cdot}7$, $k = 0{\cdot}07250$): ——— Euler CFD code; – – – FIR network output.

first case study, the overall features of the unsteady aerodynamic response are captured. Again, the lift force coefficient response of the FIR network model is better than the pitch moment response.

When tested in the linear range of the aerodynamic response, the FIR network model reveals good approximation of the lift coefficient response; however, a very poor prediction of the moment coefficient response (in the form of a large out of phase motion) can also be observed. This linear case in Figure 20, is obtained from a sinusoidal motion with mean incidence equal to zero, $0{\cdot}5^\circ$ amplitude, reduced frequency of 0·07250, and $M = 0{\cdot}7$. The FIR network model output for this case reveals a reasonable approximation of the lift

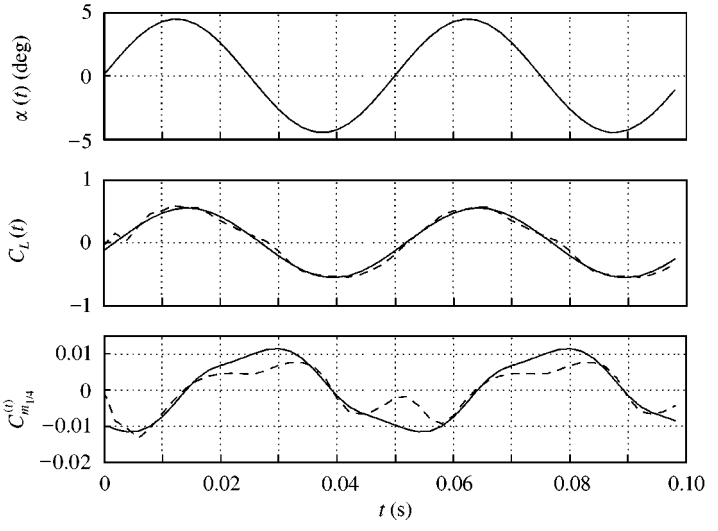

Figure 21. Generalization test of the FIR network model to arbitrary motion history (high-frequency case, $M = 0{\cdot}625$, $k = 0{\cdot}16238$): ——— Euler CFD code; – – – FIR network output.

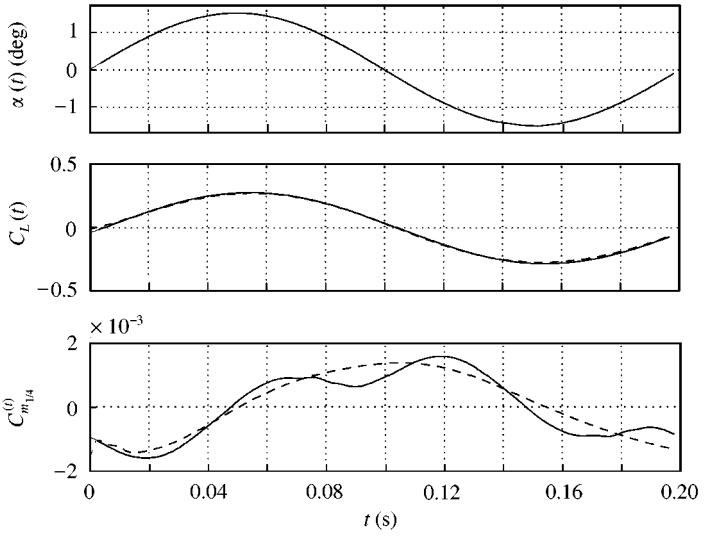

Figure 22. Generalization test of the FIR network model to arbitrary motion history (low-frequency case, $M = 0{\cdot}725$, $k = 0{\cdot}03499$): ——— Euler CFD code; – – – FIR network output.

coefficient response; however, a very poor prediction of the moment coefficient response, in the form of large out-of-phase motion, can also be observed. As in the first case study, a larger set of training patterns is required to improve the predictive qualities of the network model.

In the nonlinear range of the aerodynamic response, the FIR network for the second case study is tested for oscillatory motions (cf. Figures 21 and 22) at different frequency values compared with the ones in the training sets. The frequency for the case in Figure 21 is twice that of the training set oscillatory case, the amplitude is $4{\cdot}5^\circ$ and the Mach number is equal to 0·625. The second case in Figure 22 presents a frequency value that is half that of the

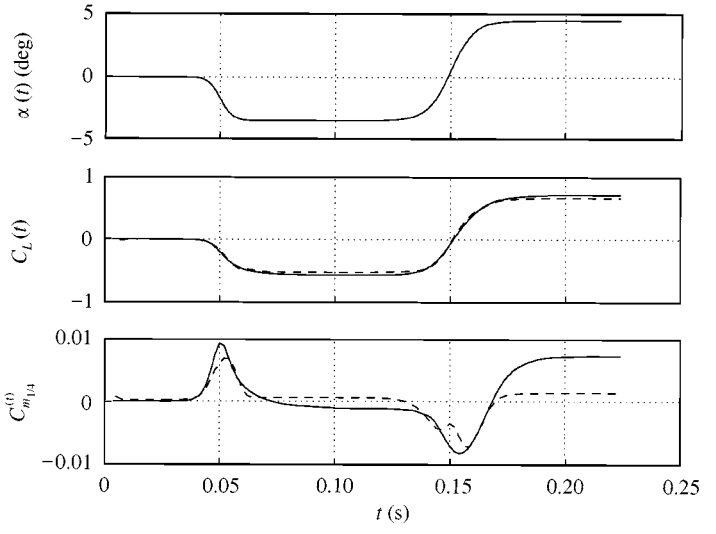

Figure 23. Generalization test of the FIR network model to arbitrary motion history ($M = 0{\cdot}65$): ——— Euler CFD code; – – – FIR network output.

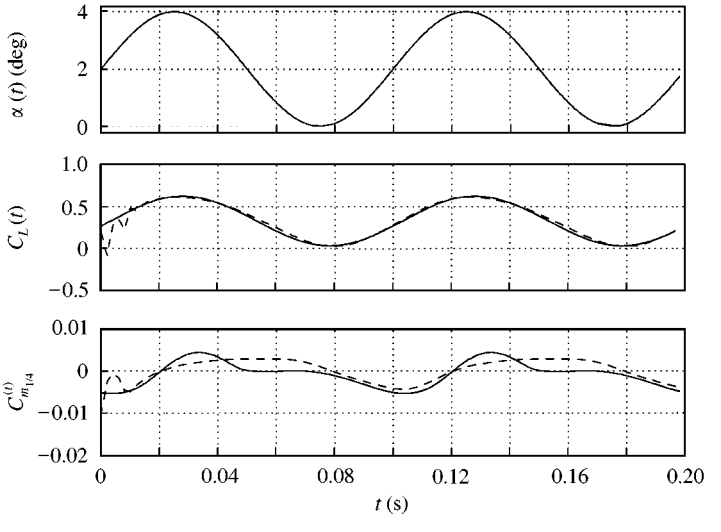

Figure 24. Generalization test of the FIR network model to arbitrary motion history ($M = 0{\cdot}65$, $k = 0{\cdot}07807$): ——— Euler CFD code; – – – FIR network output.

training set, the amplitude is 1·5° ($M = 0{\cdot}725$). The FIR network approximation of the pitch moment coefficient response for these cases, again, exhibits very poor results.

Figures 23–26 present more generalization tests of the FIR network model for the second case study. These cases correspond to pulses, ramps, and oscillatory input motions in the range of nonlinear behaviour of aerodynamic response, and for different Mach numbers that were used for training. Most of the predictive failures arise in the pitch moment responses, where larger errors can be observed. Despite the differences and the prediction disparities, the FIR network model exhibits the main features of the unsteady responses, even at Mach numbers different from those adopted in the training sets. Larger errors in the steady-state response of the pitch moment can also be observed for a range of Mach

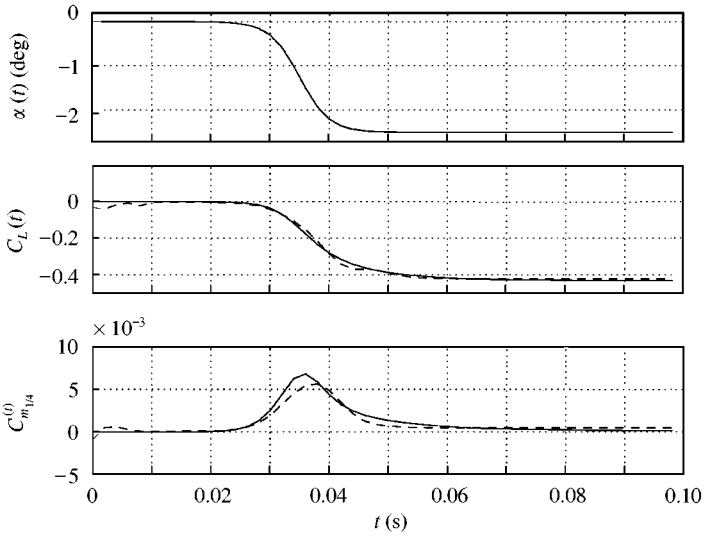

Figure 25. Generalization test of the FIR network model to arbitrary motion history ($M = 0{\cdot}68$): ——— Euler CFD code; – – – FIR network output.

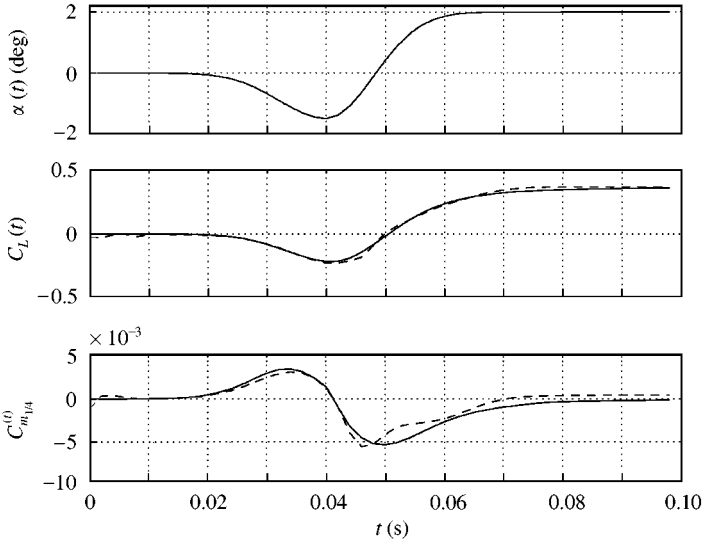

Figure 26. Generalization test of the FIR network model to arbitrary motion history ($M = 0{\cdot}7$): ——— Euler CFD code; – – – FIR network output.

numbers in which shock waves are present. As already discussed for the first case study, discrepancies in the predictions of the lift and pitch moment responses highlight the need for the improvements in the network identification algorithm and/or in the training patterns used.

The behaviour of the FIR network model is also tested for a case with Mach number beyond the training limits. An oscillatory motion with the same frequency as that used in the training sets, amplitude 1° and Mach number of $0{\cdot}75$ ($k = 0{\cdot}06766$), is considered. Figure 27 shows that the network model (in particular for the lift coefficient response) provides reasonable predictive characteristics.

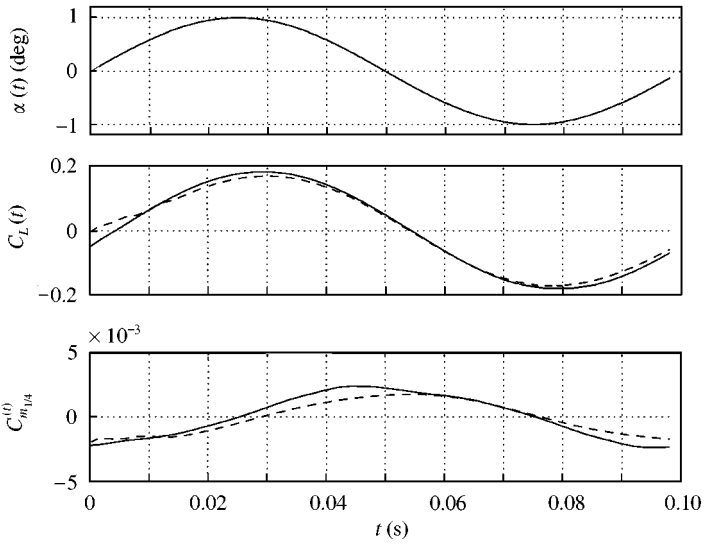

Figure 27. Generalization test of the FIR network model to a motion history beyond the training limits ($M = 0{\cdot}75$, $k = 0{\cdot}06766$): ——— Euler CFD code; – – – FIR network output.

5. CONCLUSIONS

A novel functional form, the multi-layer functional, is used to identify a model of the unsteady aerodynamic response of a 2-D aerofoil applicable to a range of Mach numbers in the transient regime. Multi-layer functionals, realized by FIR neural networks, furnish a suitable parametric model for the prediction of nonlinear motion-induced unsteady aerodynamic loads over a limited range of Mach numbers in transonic flow regime. The approach also has the advantage of intrinsically accounting for nonlinearities and time-history dependencies encountered in unsteady flow regimes. The methodology can also be used to provide multiple input multiple output models for aeroelastic applications (analysis and control design), allowing fast evaluation of the aerodynamic responses. Finally, the difficulties related to the traditional nonlinear system identification approaches are diminished by using neural network modelling schemes.

The combination of genetic search and random search to identify a FIR neural network model is shown to overcome many of the difficulties associated with the standard temporal back-propagation algorithm, facilitating the manipulation of complex network architectures and training parameters. Generalization test results show that, given only the limited training set data, the FIR neural network models are capable of reasonable predictions of the unsteady transonic aerodynamic responses due to any motion history and flow parameters within the training boundaries. Two case studies are presented where network models are identified for fixed Mach numbers and for a range of Mach numbers. Although the results for the moment coefficient response are relatively poor, good predictions of the lift force coefficient response are achieved. The generalization performance of the FIR network models reveals the importance of the features of the training patterns to the identification algorithm. The complexity of nonlinearities involved in the aerodynamic cases, added to the limitations on the information contained in the training sets available for the identification process, represent important factors in the final FIR network model.

ACKNOWLEDGEMENTS

The first author (F. Marques) acknowledges the financial support of the Brazilian Federal Research Agency, *CNPq*, during the tenure of a postgraduate research studentship and the São Paulo State Research Agency, *FAPESP*. The authors would like to acknowledge the assistance of Mr L. Dubuc, Department of Aerospace Engineering, University of Glasgow, in the preparation of the CFD aerodynamic data.

REFERENCES

BILLINGS, S. A. 1980 Identification of nonlinear systems — a survey. *IEE Proceedings D* **127,** 272–285.

CYBENKO, G. 1989 Approximation by superposition of a sigmoidal function. *Mathematics of Control, Signals, and Systems* **2,** 303–314.

DUBUC, L., CANTARINI, F., WOODGATE, M., GRIBBEN, B., BADCOCK, K. J. & RICHARDS, B. E. 1997 Solution of the Euler Unsteady Equations Using Deforming Grids. Report GU-AERO-9704, University of Glasgow.

GOLDBERG, D. E. 1989 *Genetic Algorithm in Search, Optimization, and Machine Learning*. Reading: Addison-Wesley.

HAYKIN, S. 1994 *Neural Networks — A Comprehensive Foundation*. New York: Macmillan College Publishing.

MARQUES, F. & ANDERSON, J. 1996 Modelling and identification of non-linear unsteady aerodynamic loads by neural networks and genetic algorithms. In *Proceedings of the 20th Congress of the International Council of the Aeronautical Sciences — ICAS* 96, Sorrento, Italy, Vol. 1, pp. 243–251.

MARQUES, F. 1997 Multi-layer functional approximation of non-linear unsteady aerodynamic response. Ph.D. thesis, University of Glasgow, Glasgow, Scotland, U.K.

MCCROSKEY, W. J. 1977 Some current research in unsteady fluid dynamics. *ASME Journal of Fluids Engineering* **99,** 8–39.

MCCROSKEY, W. J. 1982 Unsteady airfoils. *Annual Review of Fluid Mechanics* **14,** 285–311.

MODHA, D. S. & HECHT-NIELSEN, R. 1993 Multilayers functionals. In *Mathematical Approaches to Neural Networks* (ed. J. G. Taylor), NorthHolland Mathematical Library. Amsterdan: Elsevier.

NIXON, D. (ed.) 1989 Unsteady transonic aerodynamics. *Progress in Astronautics and Aeronautics*, Vol. 120. Washington: AIAA.

SCHETZEN, M. 1980 *The Volterra and Wiener Theories of Nonlinear Systems*. New York: John Wiley & Sons.

SILVA, W. A. 1993 Application of nonlinear systems theory to transonic unsteady aerodynamic responses. *Journal of Aircraft*, **30,** 660–668.

TIJDEMAN, H. & SEEBASS, R. 1980 Transonic flow past oscillating airfoils. *Annual Review of Fluid Mechanics* **12,** 181–222.

TOBAK, M. & CHAPMAN, G. T. 1985 Nonlinear problems in flight dynamics involving aerodynamic bifurcations. In *AGARD Symposium on Unsteady Aerodynamics*; *Fundamentals and Applications to Aircraft Dynamics*, Göttingen, Germany, paper 25.

TOBAK, M. & PEARSON, W. E. 1964 A study of nonlinear longitudinal dynamic stability. NASA TR R-209.

TOBAK, M. & SCHIFF, L. B. 1981 Aerodynamic mathematical modeling—basic concepts. *AGARD Lecture Series no*. 114, paper no. 1.

WAN, E. A. 1990 Temporal backpropagation: an efficient algorithm for finite impulse response neural networks. In 1990 *Connectionist Models Summer School* (eds D. S. Touretzky, J. L. Elman, T. J. Sejnowski & G. E. Hinton), San Mateo, Calif., U.S.A., pp. 131–137.

APPENDIX: NOMENCLATURE

$C_L(t)$	unsteady aerodynamic lift force coefficient response at time t
$C_{m_{1/4}}(t)$	unsteady aerodynamic pitch moment coefficient response at 25% chord length at time t
$d_i(n)$	desired output of training set i at discrete-time n
f	fitness function
h_j	unit impulse response of process unit j
h_{ji}	impulse response of neuron j due to excitation applied to synapse i

k	reduced frequency
L	total number of time samples per training set
$\mathscr{L}$	linear functional representation
M	Mach number
$\mathscr{MF}$	multi-layer functional representation
n	discrete-time step
N_c	number of input–output training sets
N_i^f	chromosome flag indicating whether the neuron i exists or not
P_n	probability for the mutation of a neuron value (existent or nonexistent)
P_t	probability for the mutation of a time-delay value
t	time
T_{ji}	memory span of the synapse i belonging to the neuron j
u_t	scalar generalized coordinate or displacement history
U_∞	freestream velocity
v_j	activation potential of neuron j
$w_{ji}(\tau_{ji})$	weight value of synapse i belonging to neuron j corresponding to the time-delay τ_{ji}
$x_i(t)$	excitation applied to synapse i at time t
$y(t)$	dynamic system output response at time t
$\alpha(t)$	angle of attack value at time t
α_t	angle of attack history
β	perturbation constant used to update weight and bias values
ζ	real-valued constant
θ_i	bias value of neuron i
τ_{ji}	number of time-delays of the finite memory filter in synapse i belonging to the neuron j
φ	neuron activation function defined as a nonconstant, bounded, monotone-increasing continuous function (for example, a sigmoidal function)